

Article

Effect of the Medium Composition on the Zn²⁺ Lixiviation and the Antifouling Properties of a Glass with a High ZnO Content

Leticia Esteban-Tejeda ^{1,4}, Francisco J. Palomares ¹, Belén Cabal ^{2,5}, Roberto López-Píriz ², Adolfo Fernández ^{2,*}, David Sevillano ³, Luis Alou ³, Ramón Torrecillas ² and José S. Moya ^{1,2}

¹ Institute of Materials Science of Madrid (ICMM-CSIC), Cantoblanco, 28049 Madrid, Spain; estebanl@tcd.ie (L.E.-T.); fjp@icmm.csic.es (F.J.P.); jsmoya@icmm.csic.es (J.S.M.)

² Nanomaterials and Nanotechnology Research Center (CINN), CSIC-University of Oviedo (UO), Avda de la Vega 4-6, El Entrego, 33940 San-Martín del Rey Aurelio, Spain; b.cabal@cinn.es (B.C.); lopezpiriz@gmail.com (R.L.-P.); r.torrecillas@cinn.es (R.T.)

³ Microbiology Unit, Medicine Department, Universidad Complutense, Avda. Complutense s/n, 28040 Madrid, Spain; dsevilla@med.ucm.es (D.S.); luisalou@med.ucm.es (L.A.)

⁴ School of Chemistry-CRANN, Trinity College Dublin, Green College, Dublin 2, Ireland

⁵ Nanoker Research, Pol. Ind. Olloniego, Parcela 22A, Nave 5, 33660 Oviedo, Spain

* Correspondence: a.fernandez@cinn.es; Tel.: +34-985-733-644

Academic Editor: Enrico Bernardo

Received: 23 December 2016; Accepted: 7 February 2017; Published: 13 February 2017

Abstract: The dissolution of an antimicrobial ZnO-glass in the form of powder and in the form of sintered pellets were studied in water, artificial seawater, biological complex media such as common bacterial/yeast growth media (Luria Bertani (LB), yeast extract, tryptone), and human serum. It has been established that the media containing amino acids and proteins produce a high lixiviation of Zn²⁺ from the glass due to the ability of zinc and zinc oxide to react with amino acids and proteins to form complex organic compounds. The process of Zn²⁺ lixiviation from the glass network has been studied by X-ray photoelectron spectroscopy (XPS). From these results we can state that the process of lixiviation of Zn²⁺ from the glass network is similar to the one observed in sodalime glasses, where Na⁺ is lixiviated to the media first and the fraction of Zn that acts as modifiers (~2/3) is lixiviated in second place. After the subsequent collapse of the outer surface glass layer (about 200–300 nm thick layer) the dissolution process starts again. Antifouling properties against different bacteria (*S. epidermidis*, *S. aureus*, *P. aeruginosa*, *E. coli*, and *M. lutea*) have also been established for the glass pellets.

Keywords: amino acids; Zn dispenser; biofilm; antimicrobial glass

1. Introduction

Surfaces with antifouling properties to resist the adsorption of microbes are vital in a wide range of biomedical applications, such as in catheters, prosthetic devices, contact lenses, devices for drug delivery, or patterned materials for cell culture [1–4]. Zinc oxide nanoparticles [5] are currently used to functionalize surfaces to investigate their potential ability to reduce biofilm formation on metal and polymer surfaces [6], medical implants [7], and for their oxidative photocatalytic activity to be used in waste-water treatment [8].

It is well reported in the literature that dissolution of ZnO metal oxide produces metal ions (Zn²⁺) which are known to be responsible for toxicity to bacteria. Consistently, a tight link is found between the dissolved concentration of metal in solution and the inhibition of bacterial growth [9–21]. The excess absorption of zinc prevents copper and iron absorption by cells, and furthermore Zn²⁺ acts

as a strong Lewis acid to the point of being highly corrosive [22]. It has recently been established that zinc toxicity is strongly dependent on the medium composition. Low ZnO dissolution was observed in aqueous media (Milli-Q and PBS (Phosphate-buffered saline)) without complex organic components. Conversely, dissolution about two orders of magnitude higher was detected in media with complex organic components such as amino acids and proteins (i.e., Luria Bertani (LB) and Tryptic Soy Broth (TSB)). In this sense ZnO micro/nano-particles can almost be completely dissolved in the mentioned media instantaneously. Consequently, the physical structure and the ZnO particle morphology can be strongly affected as well as their interactions with cell membranes and their ability to penetrate into cells and organisms. Moreover, Li et al. found that the generation of zinc complexes with the organic compounds from the bacterial growth media reduces the amount of free Zn^{2+} ions in solution and as a consequence, cytotoxicity drastically decreases [16].

Considering the complexity as well as the incompletely understood dissolution process of ZnO particulate and coating systems in the mentioned media in this investigation, instead of a zinc oxide system we selected a high ZnO content glass (35 wt %) which has been recently developed by the authors [23]. This glass can be considered chemically stable, non-toxic, and with an excellent activity ($>3 \log_{10}$ reduction in colony forming-units) against *E. coli* (Gram-negative), *S. aureus* (Gram-positive), and *C. krusei* (yeast). At a concentration of 2 mg/mL, this glass was also found to be biocompatible with NIH-3T3 cells (cell viability $>80\%$).

The present work is focused on studying the effect of different simple media (water and artificial seawater) and biological complex media (Luria Bertani, yeast extract, tryptone, L-glutamine, and Human Serum) on the kinetics of zinc dissolution of the selected glass. This glass was selected because of its thermal stability which implies that no devitrification takes place during the sintering process at 630 °C, therefore the glass pellets have the same amorphous structure as the starting powder. The glass dissolution was determined both for the powder and for the sintered pellets. XPS was used to study the lixiviation of the Zn ions from the glass network using sintered glass pellets before and after being immersed in LB for 40 days. The cytotoxicity and antifouling properties of this glass have also been addressed using sintered glass pellets versus bacteria (*S. epidermidis*, *M. lutea*, *S. aureus*, *P. aeruginosa*) and yeast (*C. albicans*).

2. Materials and Methods

2.1. Preparation of the Glass Powders and Pellets

A zinc-containing glass ($d_{50} = 6.3 \pm 0.1 \mu\text{m}$) belonging to the B_2O_3 - SiO_2 - Na_2O - ZnO system and with the following chemical composition (wt %): 19.29% SiO_2 ; 34.24% B_2O_3 ; 5.55% Na_2O ; 5.13% Al_2O_3 and 34.73% ZnO (labelled as ZnO35), was prepared by the fusion of mixtures of Na_2CO_3 , SiO_2 , B_2O_3 , ZnO , and Al_2O_3 in Pt crucibles at 1250 °C for 1 h in an electric furnace. After melting, it was quenched by dipping the crucible into water, dried, grinded in an agate mortar, and sieved down to 30 μm . The average particle size of the obtained powder was found to be $d_{50} = 6.3 \pm 0.1 \mu\text{m}$. The glass formulation was designed in the miscibility area according to the equilibrium diagram studied by Taylor et al. [24] and was chosen based on the high antimicrobial activity shown in a previous study [23]. Al_2O_3 was added as a stabilizer. The obtained ZnO35 glass powder was subsequently uniaxially pressed (250 MPa) to obtain green pellets and was then thermally treated for 1 h in air at 630 °C to fabricate dense glass pellets with about 10 mm diameter and 2 mm thickness. The sintering temperature was selected based on the deformation temperature of these glasses determined by hot stage microscopy. The ZnO35 pellet after immersion in LB medium is labelled as ZnO35BIO. As a reference, a non-antimicrobial window glass type pellet named G1 with the following chemical composition (wt %): 70.2% SiO_2 , 15.8% Na_2O , 7.1% CaO , 3.2% MgO and 1.06% B_2O_3 , was used.

2.2. Characterization of the Glass Powders and Pellets

The ZnO35 starting powders were fully characterized by: Nuclear Magnetic Resonance (NMR), particle size, X-ray diffraction (XRD), Transmission electron microscopy (TEM), Differential thermal analysis (DTA), and hot stage microscopy in a previous work [23]. The glass pellets were characterized by X-ray diffraction (XRD) using a Bruker D8 diffractometer with CuK radiation working at 40 kV and 30 mA in a step-scan spectroscopy. X-ray photoelectron spectroscopy (XPS) measurements were performed in an ultrahigh vacuum (UHV) chamber with a base pressure of 10^{-9} mbar using a hemispherical electron energy analyzer (SPECS Phoibos 150 spectrometer), and non-monochromatized radiation ($K\alpha$ 1486.6 eV) from an Al X-ray source operated at 200 W to minimize sample charging effects. XPS spectra were recorded at a normal emission take-off angle using an energy step and pass-energy of 0.1 eV and 20 eV for core level spectra and of 0.5 eV and 40 eV for survey scans, respectively [25]. Samples were irradiated with low energy Ar^+ ions for depth profiling experiments.

2.3. Lixiviation of Zn^{2+}

The release of Zn^{2+} from the zinc containing glasses was evaluated in seven different media: (i) distilled water; (ii) water containing 3 wt % NaCl (artificial seawater); (iii) Luria Bertani (LB) medium; (iv) L-Glutamine; (v) Tryptone; (vi) Yeast Extract; and (vii) Human Serum. An aqueous suspension (5 mg/mL) of ZnO containing glass powder in the corresponding media was kept under agitation at a constant rate of 120 rpm during 24 h at 37 °C. These conditions were kept for all the experiments in the different media. The analysis of zinc was performed by Inductively Coupled Plasma (ICP) using a Perkin Elmer optical emission spectrometer model Optima 2100 DV. The solutions analysed by ICP were previously centrifuged and filtered in order to obtain an aqueous solution containing the metal ions free of glass particles.

2.4. Biofilm Study

2.4.1. Microorganisms and Growth Conditions

Five bacterial species, including three Gram-positive strains (*Staphylococcus epidermidis* ATCC 35984, *S. aureus* ATCC 29213, and *Micrococcus lutea* ATCC 9341), two Gram-negative strains (*Escherichia coli* ATCC 25922 and *Pseudomonas aeruginosa* ATCC 23389), and the yeast *Candida albicans* ATCC 64548, were studied as representative microorganisms involved in biofilm formation on inert substrates. The selected microorganisms are responsible for >95% of infections related with permanent devices used in clinical practices. All strains were purchased from American Type Culture Collection and were strong biofilm producers as determined spectrophotometrically by the crystal violet staining method [26,27] on polystyrene flat-bottom 96-well microtiter plates (Greiner bio-one, Kremsmünster, Austria) (data not shown).

Bacterial colonies from a fresh culture on Columbia agar (BD, Becton, Dickinson and Co., Sparks, MD, USA), were grown overnight in an orbital shaker (100 rpm) at 37 °C in Tryptic Soya broth (TSB, BD) supplemented with 50 mM glucose (TSB-glu, Sigma, St. Louis, MI, USA). Cells were harvested, washed twice in phosphate-buffered saline (PBS, Sigma), and adjusted to a 1×10^7 cell/mL concentration in TSB-glu. *C. albicans* were grown in Sabouraud-dextrose agar (BD), propagated overnight at 37 °C in Yeast Nitrogen Base medium (YNB, BD) supplemented with 50 mM glucose (YNB-glu), and adjusted to 1×10^7 cell/mL concentration.

2.4.2. Biofilm Formation Assays

Biofilms were formed on the surface of the glass pellets using a static in vitro model. Prior to biofilm production, pellets were autoclaved, incubated in human serum for 12 h, and washed twice with TSB-glu or YNB-glu. The pellets were incubated in 12-well tissue culture plates (Greiner bio-one) for 90 min at 37 °C with 3 mL of the standardized culture of each microorganism (adhesion phase).

Pellets were then washed with 5 mL of PBS to remove unattached planktonic cells, placed into new wells of the culture plates, and incubated for 24 h, 48 h, and 5 days in TSB-glu or YNB-glu.

2.4.3. Biofilm Quantification

After biofilm formation, the pellets were singly placed in 0.3 mL of PBS. Pellets were vigorously vortexed for 1 min, followed by sonication at 37 KHz (Fisherbrand 15050, Thermo Fisher Scientific, Waltham, MA, USA) for 10 min and by 1 min of vortexing, to ensure the complete extraction of the biofilm cells. The suspensions obtained were diluted prior to seeding onto Columbia agar or Sabouraud-dextrose agar plates, using a spiral platter workstation (Don Whitley Scientific, Shipley, UK). The plates were incubated for 48 h at 37 °C prior to counting colony forming units (CFU). Results were expressed as CFU/mL. All experiments were performed at least five times.

The antimicrobial effect of ZnO was measured by the reduction in percentage, (R%), of the number of viable cells recovered from the ZnO35 pellets in comparison to the number of viable cells recovered from the control G1 pellets after 24 h, 48 h, and 5 days of biofilm development. R% was calculated using $R\% = 100 - (100 \times I_{ZnO})/I_{G1}$, where I_{ZnO} is the number of viable counts (CFU/mL) in ZnO35 pellets, and I_{G1} is the number of viable counts (CFU/mL) in G1 pellets.

2.4.4. Scanning Electron Microscopy (SEM)

S. epidermidis and *E. coli* biofilms formed on the glass pellets were fixed with a solution of 2.5% glutaraldehyde and 4% paraformaldehyde (Thermo Fisher Scientific). After 1 h of incubation at room temperature, samples were dehydrated with a graded series of ethanol, immersed in hexamethyldisilazane, and dried with CO₂ in a critical point dryer (Balzers CPD 030, Schalksmühle, Germany). The specimens were coated with gold/palladium and visualized in a scanning electron microscope (JEOL JSM 6400; Tokyo, Japan).

2.4.5. Statistical Analysis

Comparisons of cell burdens on G1 or ZnO35 pellets among maturation stages were performed using analysis of variance (ANOVA) with the Tukey's test for multiple comparisons (GraphPad Prism software v. 5.2, San Diego, CA, USA). Comparisons between the number of viable cells recovered from the G1 and ZnO pellets were explored by using the Student's *t* test (two-tailed *t*-test). A *p*-value < 0.05 was considered significant.

3. Results and Discussion

3.1. Characterization of the Glass Pellets

The XRD patterns corresponding to the starting glass powders and the subsequently obtained pellets are shown in Figure 1. The starting glass powders as well as the pellets show the characteristic bell curve for amorphous glasses with the maximum located at $2\theta \sim 30^\circ$ in both cases.

The XRD band located at $\sim 30^\circ$ may correspond to the most intense XRD diffraction peak (113) of the Willemite (α -Zn₂SiO₄) phase (JCPDS file 37-1485) [28].

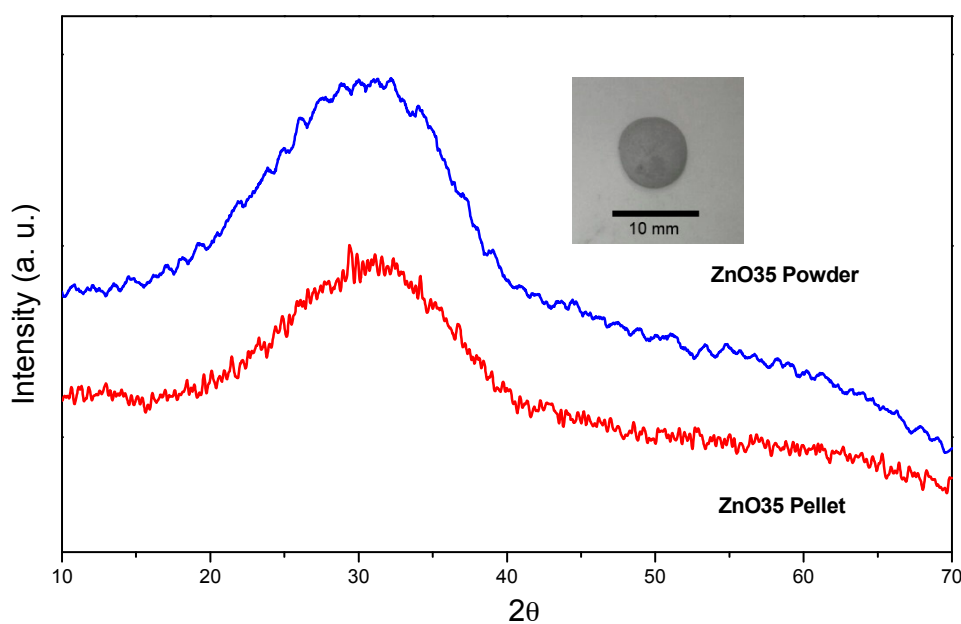


Figure 1. XRD patterns of the starting glass powders of ZnO35 and the obtained ZnO35 sintered pellets at 630 °C (insert photograph of ZnO35 pellet).

3.2. Chemical Stability: Lixiviation of Zn²⁺

The chemical stability in terms of the Zn²⁺ release from ZnO35 powders and pellets was analysed in different media to define their use in biomedical applications such as catheters, stents, implanted devices, and prostheses. Both the glass and the powders showed high antimicrobial activity against bacterial species and to a lesser extent against yeast as already reported in a previous study [23]. In that preliminary study, the non-cytotoxicity of this material was also proven for the concentration (5 mg/mL) used in the present investigation.

Table 1 reports the amount of zinc released from the ZnO35 powder to different media after 24 h. All biological complex media containing amino acids (LB, yeast extract, L-Glutamine 0.5 wt % and Human Serum) produce a high release of Zinc, while the simple media do not significantly affect zinc lixiviation which remains very low (~0.5 ppm). It is relevant to point out that these values are about two orders of magnitude smaller than the previous ones.

Table 1. Zn²⁺ released from the ZnO35 powder to the media after 24 h.

Medium	Zn ²⁺ (ppm)	SD
Distillate Water	0.5	0.01
Water sea-like (3 wt % NaCl)	0.47	0.01
Luria Bertani (LB)	126.3	0.06
Yeast Extract (0.5 wt %)	192.681	0.06
L-Glutamine (0.5 wt %)	386.6	0.06
Human Serum	248.99	0.05

The same tendency is observed for the pellets. The lixiviation in distilled water and artificial seawater was <1 ppm after 40 days for the ZnO35 pellets (data not shown).

It is well reported that amino acids and peptides form organic complexes with zinc and zinc oxide, resulting in zinc lixiviation. Liu et al. studied the reactions and rates of solubility of ZnO thin film coatings exposed to different bacterial growth media [29]. They observed that over a 24 h period, 10- to 30-fold higher concentrations of soluble zinc were detected in LB media, relative to those not containing complex organic, PBS, and Milli-Q water. Therefore, zinc lixiviation may be dependent

on the concentration of amino acids in the media. In order to rationalize this statement and with the purpose of determining the amount of zinc released from the glass, ZnO35 pellets were introduced into media containing different concentrations of amino acid L-glutamine (0.05, 0.125 and 0.5 wt %) for 24 h.

Figure 2 shows almost a linear fit between the L-Glutamine concentration and the Zn^{2+} release. These results strongly suggest that the concentration of free amino acids is the factor that determines the zinc release to the organic media. All biological complex media used in these experiments (Table 1) were previously sterilized by an autoclave at 120 °C for 1 h. Due to the sterilization process, the proteins contained in these media were partially or even completely disrupted from their former amino acids, therefore all these media contain a high amount of free amino acids and peptides which explains the high release of zinc.

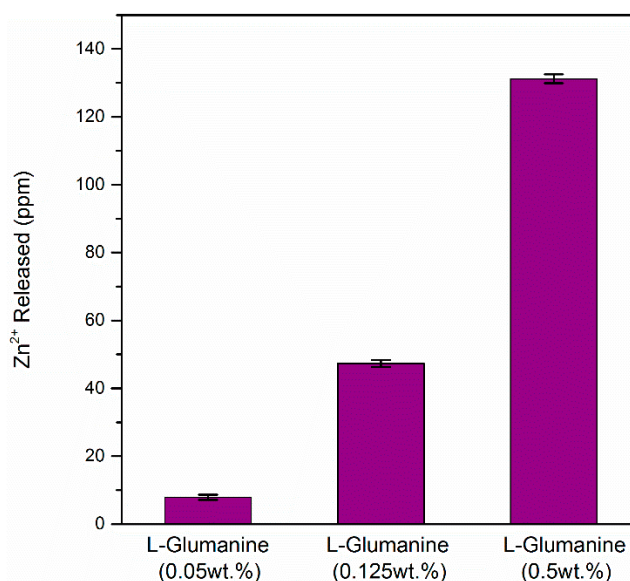


Figure 2. Zinc released from the ZnO35 pellet after 24 h in different concentrations of L-Glutamine.

3.3. X-ray Photoelectron Spectroscopy Study

The XPS experiments have been performed to study the chemical composition of the samples in the range of 100 nm upon consecutive cycles of ion bombardment with low energy Ar^+ ions of the ZnO35 pellet before and after being immersed in LB medium (1 wt % tryptone; 0.5 wt % yeast extract; 1 wt % NaCl; and 1.5 wt % agar) at 30 °C for 40 days, labelled as ZnO35 and ZnO35BIO, respectively.

Figure 3 displays a set of Si2p, Zn3p, Al2p, and Na2s core level emissions. Upon analysis of the corresponding XPS spectra, a strong reduction in the intensity of both Na2s and Zn2p peaks in the ZnO35BIO sample is observed, which reveals a significant depletion of Na and Zn (Figure 3A). It is worth mentioning that sodium is a network modifier and, as such, it is expected to be released to the medium, considering that the modifiers are the first elements of the glass network to be released [30]. In the case of zinc, lixiviation to the media also takes place, but at a lower degree compared to the one corresponding to sodium. This result suggests that there are two different types of zinc in the glassy matrix network: (i) as a former ion that is kept inside the glass network in tetrahedral positions [23] similar to Si^{4+} , B^{3+} , Al^{3+} and (ii) as a network modifier that is lixiviated as a consequence of the presence of high amounts of amino acids in the medium.

Consecutive ion bombardment cycles with low energy Ar^+ ions (1 keV) were carried out to obtain in-depth chemical information of the ZnO35 and ZnO35BIO samples. In both cases, the line shape and intensity of the XPS spectra resemble steady over ion sputtering steps within the first 100 nm. The analysis of the XPS spectra evolution shows that the ratios Zn/Si and Na/Si keep constant for

each sample. A depletion of Na and Zn also exists in the BIO sample that remains stable in a 100 nm deep layer while the sample is eroded by ion sputtering.

In addition, Figure 3B shows the XPS signals normalized to the Si2p peak. A slight difference in the intensity of the Al2p peak exists which suggests that a small fraction of Al³⁺ in the tetrahedral position has been lixiviated with the Na⁺ as a consequence of its lower stability in the glass network compared to tetrahedral Si⁴⁺.

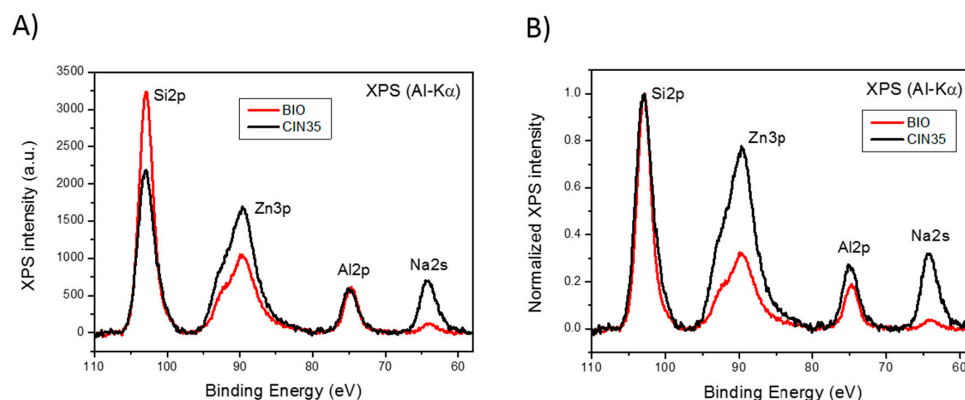


Figure 3. X-ray photoelectron spectroscopy (XPS) spectra in the Si2p, Zn3p, Al2p, and Na2s region of the ZnO35 pellet and the ZnO35 pellet after being immersed for 40 days in LB (labelled as BIO). (A) XPS signals upon background subtraction; (B) signals normalized to the Si2p peak upon background subtraction.

In summary, from these results we can state that the process of lixiviation of Zn²⁺ from the glass network is similar to the one observed in sodalime glasses, where Na⁺ is lixiviated to the media first and the fraction of Zn acts as a modifier, ~2/3 considering the area ratio under the peaks (Figure 3B), is lixiviated in second place. After the subsequent collapse of the outer surface glass layer (about 200–300 nm thick), the dissolution process started again [23]. This process is completely different from the results reported by Liu et al. [29] for zinc oxide thin films, which show that in less than 10 h, i.e., in LB, the thin film had almost completely dissolved in the media.

On the contrary, in our particular case the glass is an excellent dispenser of Zn²⁺ to the media for a very long period of time, in the range of years.

3.4. Antimicrobial Activity

In Figures 4 and 5 the evolution of viable cells within biofilms on control G1 pellets and ZnO35, respectively, are shown.

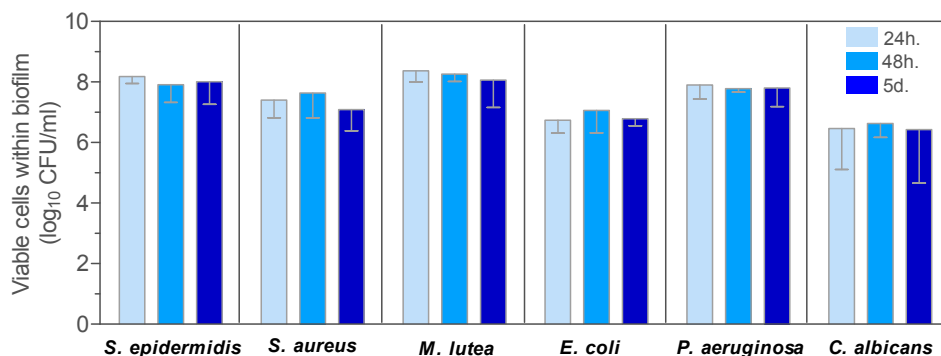


Figure 4. Evolution of viable cells within biofilms developed for 24 h, 48 h, or 5 days on control G1 pellets.

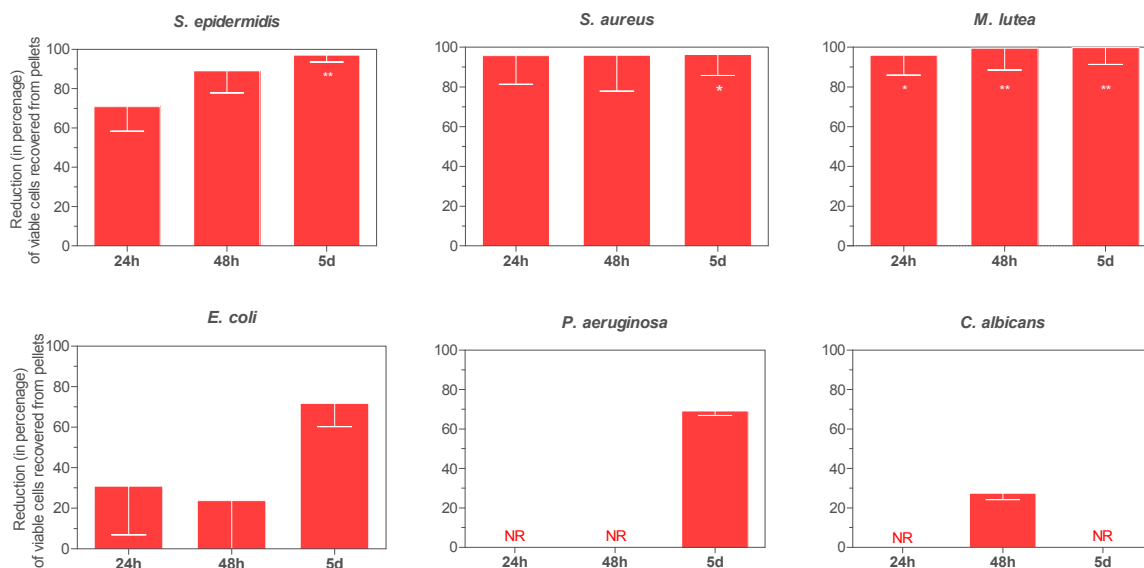


Figure 5. Effect of ZnO35 on the viability of bacterial and yeast biofilms. NR; no reduction. * $p < 0.05$, ** $p < 0.01$.

The effect of ZnO35 on the development of bacterial and yeast biofilms was studied. The G1 pellet composed of a non-antimicrobial window glass [31] was used as a control (Figure 4).

Despite some interspecies differences in the ability to form biofilms, biofilm cell loads harvested from G1 pellets were not significantly different, irrespective of the maturation age of the biofilms: 24 h, 48 h, or 5 days (Figure 4). The mean number of viable cells within the biofilm for all species after 24 h and 5 days of biofilm development ranged from 2.88×10^6 to 2.37×10^8 CFU/mL and from 2.72×10^6 to 6.30×10^7 CFU/mL, respectively.

Zinc-containing pellets decreased biofilm formation in comparison to G1 controls. As shown in Figure 5, the antibiofilm effect exerted by ZnO35 was species-dependent and increased in a time-dependent manner. Reductions in biofilm cell load increased from 24 h to 5 days for all species and significantly so for *P. aeruginosa* ($p = 0.006$). After 5 days, biofilm burdens of Gram-positive bacteria were strongly reduced by 97.1% ($p = 0.0011$), 99.8% ($p = 0.0083$), and 96.4% ($p = 0.0189$) for *S. epidermidis*, *M. lutea*, and *S. aureus*, respectively; moderately reduced for *E. coli*, 71.8%, and *P. aeruginosa*, 61.2%, and virtually not reduced for the yeast, *C. albicans*.

The SEM images confirmed biofilm formation and strongly supported the antibiofilm effect of ZnO35 (Figure 6). Small clusters of cells, which did not aggregate to form complex biofilm structures (panel C), or multilayered cell clusters (panels E and F), were observed to be patchily distributed on the surface of ZnO35 pellets instead of multi-layered three-dimensional structures formed on G1 pellets, after 24 h of biofilm development. As shown in panel 6E, zinc oxide induced cell filamentation in *E. coli* confers certain survival advantages as previously reported by Gunawan et al. [32]. Images after 5 days revealed sparsely colonized surfaces by microorganisms (panels D and G), abundant cellular debris, and seriously damaged cellular structures (panels D and H).

Results suggest that the effect is based on the generation of reactive oxygen species (ROS) in all of the tested streams, induced by the penetration of ZnO or Zn^{2+} into the cells. It also agrees with the non-cytotoxicity of this material due to the inherent resistances of eukaryotic cells towards oxidative stress [13–15,17,19]. According to the conditions tested, it can be stated that the effect of Zn based glass is bacteriostatic. However, an increase in the exposition time or a pre-activation of Zn lixiviation could lead to a bactericidal effect.

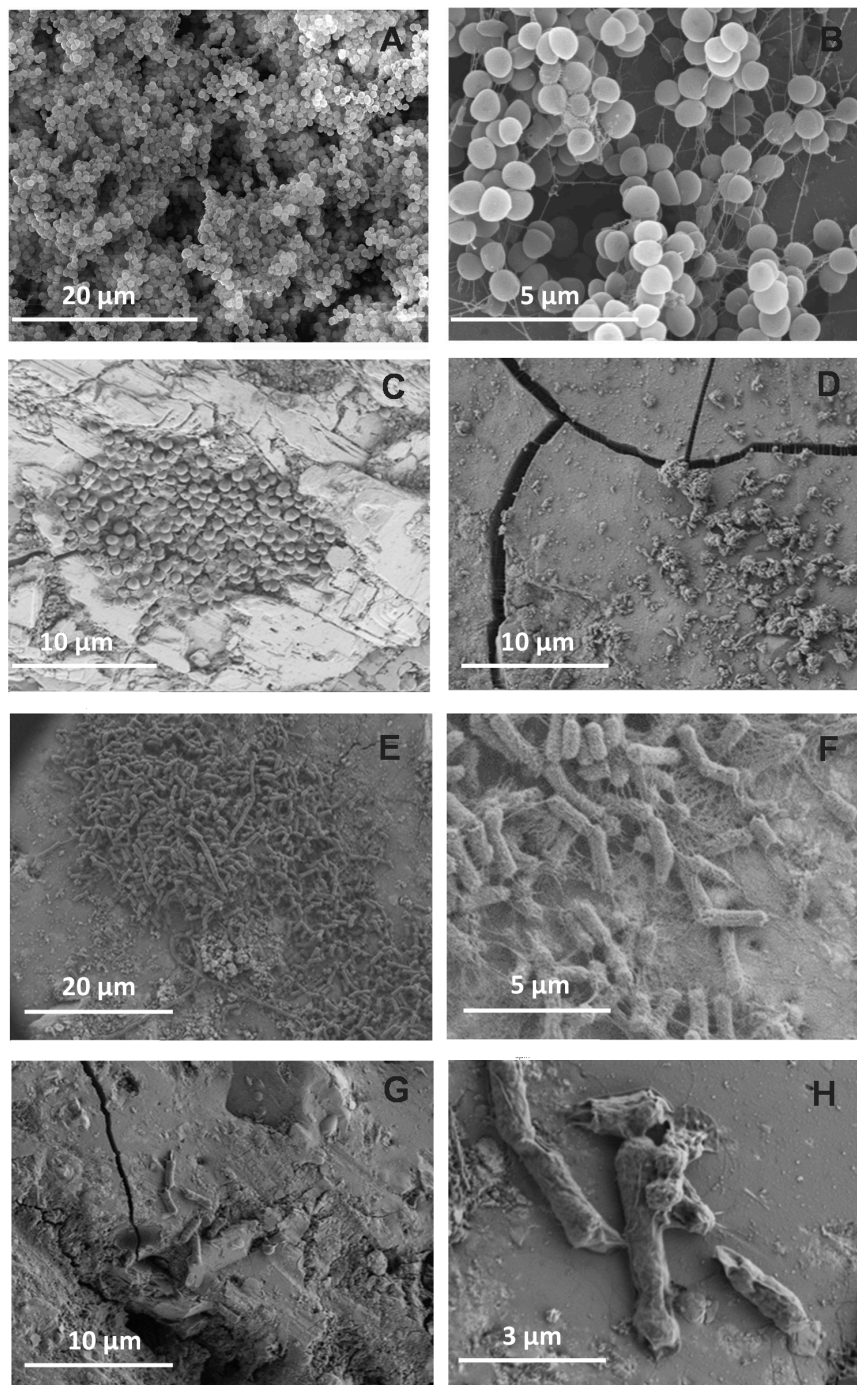


Figure 6. Scanning electron micrographs of *S. epidermidis* (A–D) and *E. coli* (E–H) grown on glass pellets. (A,B) panels show *S. epidermidis* biofilm formation on the surface of control G1 at day 5; (C,D) show colonization of ZnO35 pellets by *S. epidermidis* after 24 h (C) and 5 days (D); (E,F) show growth of *E. coli* on ZnO35 surfaces after 24 h, and (G,H) after 5 days.

In previous studies, the cytotoxicity of these glasses was evaluated for both powders and coatings using NIH-3T cells and the viability was >80% in all cases, which implies no cytotoxicity [23,33]. Considering the results obtained in this study, we can ensure that the glass shows excellent multifunctional performances as a bactericide agent and inhibits biofilm formation without cytotoxicity, which paves the way for major biomedical applications, i.e., dental care. Oral biofilms are strongly associated to the aetiology of periodontal diseases, dental caries, pulpal diseases, apical periodontitis,

peri-implant diseases, and candidosis. Furthermore, oral biofilm-associated diseases may affect systemic health through spreading infections to adjacent tissues and spaces, hematogenously disseminating oral biofilm bacteria, or inflammatory mechanisms [34]. Controlling coccoid microbiota growth is a key point to prevent oral biofilm formation and maturation around teeth and dental implants, since they are the first colonizers. Furthermore, dental caries are caused by Gram-positive cocci such as *Streptococcus mutans* and *S. sobrinus*. ZnO glasses have shown an excellent antibacterial action against Gram-positive cocci. Coating abutments with ZnO glass or doping dental fillers with ZnO glass powder would deliver an antimicrobial effect to where it most matters, in order to prevent oral biofilm formation and dental diseases.

Infections of bare intravascular metal stents are mainly caused by *S. aureus*. This situation often leads to emergency surgery with a mortality rate of up to 32.5% (non coronary: 22.9%; and coronary: 48.3%) [35]. A strategy to endow metal stents with antibacterial properties would reduce this major medical complication and save lives. The results presented in this study show ZnO glass powder and pellets as good choices for preventing Gram-positive biofilm formation. Metal stents could be coated with ZnO glasses instead of being bare, but further studies are needed to determine the expansive properties that the Ni-Ti composition provide to stents with the glass coating mechanical properties.

Periprosthetic joint infection (PJI) is estimated at 1% for hip arthroplasties and ranges between 1% and 2% for knee arthroplasties; recent data suggest that infection rates might be higher ($\geq 2\%$) than previously reported [36,37]. PJI is difficult to cure with antimicrobials and the implant often has to be removed [37]. Staphylococci (*S. aureus* and *S. epidermidis*) are the most frequently reported causes of PJIs and of concern are PJIs caused by methicillin-resistant strains that result in significant morbidity and costs for health care delivery [38]. Methicillin-resistance among staphylococci is on rise and the development of drugs with new mechanisms of action is demanded. A bactericidal effect based on the ion action of Zn^{2+} is much more efficient because bacteria cannot develop any mechanism of resistance towards it. In addition, ZnO glasses have shown a particular bactericidal action against Gram-positive cocci such as *S. aureus*. Based on the above-mentioned reasons, coating orthopedic prostheses with ZnO glass would be a strategy that could decrease patient morbidity and mortality, since it might prevent periprosthetic infection. Providing arthroplasties with an antibacterial ZnO coating would also reduce the need of antibiotic consumption and its impact on bacterial ecology.

4. Conclusions

These results suggest that the bacterial growth media strongly affects zinc dissolution from the glass matrix which has important implications on antibacterial activity and cytotoxicity. In contrast to ZnO coatings or ZnO micro/nanoparticles, this glass acts as a dispenser of Zn^{2+} ions to a media containing monoacids. These glasses have high antifouling properties against bacteria. As a consequence, this study opens up the future applicability of these glasses in a wide panoply of biomedical devices (i.e., catheters, stents, dental devices, and prostheses) where antifouling properties besides biocompatibility are required.

The chemical properties of this glass material and its surface stability are essential to fulfil the expected performances during exposure to bacteria and during interaction with the BIO media.

Acknowledgments: FJP acknowledges the support from the “Ministerio de Ciencia e Innovacion” (MICINN, Spain) through the grant MAT2016-80394-R. Belén Cabal acknowledges financial support from Jovellanos program (IDEPA, cofounded by FEDER).

Author Contributions: J.S.M. and R.T. conceived and designed the experiments, L.E.-T. performs the glass synthesis and chemical tests, D.S. and L.A. performed the antibacterial and biofilm tests, F.J.P. performed the XPS tests, B.C., R.L.-P., A.F. analyzed the data and J.S.M., R.T., F.J.P., D.S., L.A., B.C., R.L.-P., A.F. and L.E.-T. wrote the paper.

Conflicts of Interest: The authors declare no conflict of interest.

References

1. Banerjee, I.; Pangule, R.C.; Kane, R.S. Antifouling Coatings: Recent Developments in the Design of Surfaces That Prevent Fouling by Proteins, Bacteria, and Marine Organisms. *Adv. Mater.* **2011**, *23*, 690–718. [[CrossRef](#)] [[PubMed](#)]
2. Kane, R.S.; Deschatelets, P.; Whitesides, G.M. Kosmotropes Form the Basis of Protein-Resistant Surfaces. *Langmuir* **2003**, *19*, 2388–2391. [[CrossRef](#)]
3. Page, K.; Wilson, M.; Parkin, I.P. Antimicrobial surfaces and their potential in reducing the role of the inanimate environment in the incidence of hospital-acquired infections. *J. Mater. Chem.* **2009**, *19*, 3819–3831. [[CrossRef](#)]
4. Park, K.D.; Kim, Y.S.; Han, D.K.; Kim, Y.H.; Lee, E.H.B.; Suh, H.; Choi, K.S. Bacterial adhesion on PEG modified polyurethane surfaces. *Biomaterials* **1998**, *19*, 851–859. [[CrossRef](#)]
5. Kołodziejczak-Radzimska, A.; Jesionowski, T. Zinc Oxide—From Synthesis to Application: A Review. *Materials* **2014**, *7*, 2833–2881. [[CrossRef](#)]
6. Seil, J.T.; Webster, T.J. Reduced Staphylococcus aureus proliferation and biofilm formation on zinc oxide nanoparticle PVC composite surfaces. *Acta Biomater.* **2011**, *7*, 2579–2584. [[CrossRef](#)] [[PubMed](#)]
7. Colon, G.; Ward, B.C.; Webster, T.J. Increased osteoblast and decreased Staphylococcus epidermidis functions on nanophase ZnO and TiO₂. *J. Biomed. Mater. Res. Part A* **2006**, *78*, 595–604. [[CrossRef](#)] [[PubMed](#)]
8. Chan, S.H.S.; Wu, T.Y.; Juan, J.C.; Teh, C.Y. Recent developments of metal oxide semiconductors as photocatalysts in advanced oxidation processes (AOPs) for treatment of dye waste-water. *J. Chem. Technol. Biotechnol.* **2011**, *86*, 1130–1158. [[CrossRef](#)]
9. Buerki-Thurnherr, T.; Xiao, L.; Diener, L.; Arslan, O.; Hirsch, C.; Maeder-Althaus, X.; Grieder, K.; Wampfler, B.; Mathur, S.; Wick, P.; et al. In vitro mechanistic study towards a better understanding of ZnO nanoparticle toxicity. *Nanotoxicology* **2013**, *7*, 402–416. [[CrossRef](#)] [[PubMed](#)]
10. Reed, R.B.; Ladner, D.A.; Higgins, C.P.; Westerhoff, P.; Ranville, J.F. Solubility of nano-zinc oxide in environmentally and biologically important matrices. *Environ. Toxicol. Chem.* **2012**, *31*, 93–99. [[CrossRef](#)] [[PubMed](#)]
11. Chevallet, M.; Veronesi, G.; Fuchs, A.; Mintz, E.; Michaud-Soret, I.; Deniaud, A. Impact of labile metal nanoparticles on cellular homeostasis. Current developments in imaging, synthesis and applications. *Biochim. Biophys. Acta Gen. Subj.* **2016**. [[CrossRef](#)] [[PubMed](#)]
12. Xia, T.; Kovoichich, M.; Liong, M.; Mädler, L.; Gilbert, B.; Shi, H.; Yeh, J.I.; Zink, J.I.; Nel, A.E. Comparison of the mechanism of toxicity of zinc oxide and cerium oxide nanoparticles based on dissolution and oxidative stress properties. *ACS Nano* **2008**, *2*, 2121–2134. [[CrossRef](#)] [[PubMed](#)]
13. Song, W.; Zhang, J.; Guo, J.; Zhang, J.; Ding, F.; Li, L.; Sun, Z. Role of the dissolved zinc ion and reactive oxygen species in cytotoxicity of ZnO nanoparticles. *Toxicol. Lett.* **2010**, *199*, 389–397. [[CrossRef](#)] [[PubMed](#)]
14. Xie, Y.; He, Y.; Irwin, P.L.; Jin, T.; Shi, X. Antibacterial activity and mechanism of action of zinc oxide nanoparticles against *Campylobacter jejuni*. *Appl. Environ. Microbiol.* **2011**, *77*, 2325–2331. [[CrossRef](#)] [[PubMed](#)]
15. Li, J.; Liu, X.; Zhang, Y.; Tian, F.; Zhao, G.; Yu, Q.; Jiang, F.; Liu, Y. Toxicity of nano zinc oxide to mitochondria. *Toxicol. Res.* **2012**, *1*, 137–144. [[CrossRef](#)]
16. Li, M.; Zhu, L.; Lin, D. Toxicity of ZnO Nanoparticles to *Escherichia coli*: Mechanism and the Influence of Medium Components. *Environ. Sci. Technol.* **2011**, *45*, 1977–1983. [[CrossRef](#)] [[PubMed](#)]
17. Dwivedi, S.; Wahab, R.; Khan, F.; Mishra, Y.K.; Musarrat, J.; Al-Khedhairi, A.A. Reactive oxygen species mediated bacterial biofilm inhibition via zinc oxide nanoparticles and their statistical determination. *PLoS ONE* **2014**, *9*, e111289. [[CrossRef](#)] [[PubMed](#)]
18. Ma, H.; Williams, P.L.; Diamond, S.A. Ecotoxicity of manufactured ZnO nanoparticles—A review. *Environ. Pollut.* **2013**, *172*, 76–85. [[CrossRef](#)] [[PubMed](#)]
19. Padmavathy, N.; Vijayaraghavan, R. Enhanced bioactivity of ZnO nanoparticles—An antimicrobial study. *Sci. Technol. Adv. Mater.* **2008**, *9*, 035004. [[CrossRef](#)] [[PubMed](#)]
20. Sirelkhatim, A.; Mahmud, S.; Seeni, A.; Kaus, N.H.M.; Ann, L.C.; Bakhori, S.K.M.; Hasan, H.; Mohamad, D. Review on Zinc Oxide Nanoparticles: Antibacterial Activity and Toxicity Mechanism. *Nano-Micro Lett.* **2015**, *7*, 219–242. [[CrossRef](#)]

21. Rousk, J.; Ackermann, K.; Curling, S.F.; Jones, D.L. Comparative Toxicity of Nanoparticulate CuO and ZnO to Soil Bacterial Communities. *PLoS ONE* **2012**, *7*, e34197. [[CrossRef](#)] [[PubMed](#)]
22. Fukui, H.; Horie, M.; Endoh, S.; Kato, H.; Fujita, K.; Nishio, K.; Komaba, L.K.; Maru, J.; Miyauhi, A.; Nakamura, A.; et al. Association of zinc ion release and oxidative stress induced by intratracheal instillation of ZnO nanoparticles to rat lung. *Chem. Biol. Interact.* **2012**, *198*, 29–37. [[CrossRef](#)] [[PubMed](#)]
23. Esteban-Tejeda, L.; Prado, C.; Cabal, B.; Sanz, J.; Torrecillas, R.; Moya, J.S. Antibacterial and antifungal activity of ZnO containing glasses. *PLoS ONE* **2015**, *10*, e0136490. [[CrossRef](#)] [[PubMed](#)]
24. Taylor, P.; Owen, D.G. Liquid Immiscibility in the System Na₂O-ZnO-B₂O₃-SiO₂. *J. Am. Ceram. Soc.* **1981**, *64*, 360–367. [[CrossRef](#)]
25. Palomares, F.J.; Paz, E.; Soria, F.; Moya, J.S.; Burianek, M.; Muehlberg, M.; Schneider, H. Surface Chemistry of Ion Irradiated and Heat-Treated Mullite-Type Bi₂Ga₄O₉ Single Crystals. *J. Am. Ceram. Soc.* **2009**, *92*, 2993–2998. [[CrossRef](#)]
26. Feoktistova, M.; Geserick, P.; Leverkus, M. Crystal Violet Assay for Determining Viability of Cultured Cells. *Cold Spring Harb. Protoc.* **2016**, *2016*. [[CrossRef](#)] [[PubMed](#)]
27. Maestre, J.R.; Aguilar, L.; Mateo, M.; Giménez, M.J.; Méndez, M.M.; Alou, L.; Granizo, J.J.; Prieto, J. In vitro interference of tigecycline at subinhibitory concentrations on biofilm development by *Enterococcus faecalis*. *J. Antimicrob. Chemother.* **2012**, *67*, 1155–1158. [[CrossRef](#)] [[PubMed](#)]
28. López-Píriz, R.; Solá-Linares, E.; Rodríguez-Portugal, M.; Malpica, B.; Díaz-Güemes, I.; Enciso, S.; Esteban-Tejeda, L.; Cabal, B.; Granizo, J.J.; Moya, J.S.; et al. Evaluation in a dog model of three antimicrobial glassy coatings: Prevention of bone loss around implants and microbial assessments. *PLoS ONE* **2015**, *10*, e0140374. [[CrossRef](#)] [[PubMed](#)]
29. Liu, S.; Killen, E.; Lim, M.; Gunawan, C.; Amal, R. The effect of common bacterial growth media on zinc oxide thin films: Identification of reaction products and implications for the toxicology of ZnO. *RSC Adv.* **2014**, *4*, 4363–4370. [[CrossRef](#)]
30. Esteban-Tejeda, L.; da Silva, A.C.; Mello-Castanho, S.R.; Pacharroman, C.; Moya, J.S. Kinetics of dissolution of a biocide soda-lime glass powder containing silver nanoparticles. *J. Nanopart. Res.* **2013**, *15*, 1447. [[CrossRef](#)]
31. Moya, J.S.; Esteban-Tejeda, L.; Pecharromán, C.; Mello-Castanho, S.R.H.; da Silva, A.C.; Malpartida, F. Glass powders with a high content of calcium oxide: A step towards a “green” universal biocide. *Adv. Eng. Mater.* **2011**, *13*, B256–B260. [[CrossRef](#)]
32. Gunawan, C.; Teoh, W.Y.; Ricardo; Marquis, C.P.; Amal, R. Zinc Oxide Nanoparticles Induce Cell Filamentation in *Escherichia coli*. *Part. Part. Syst. Charact.* **2013**, *30*, 375–380. [[CrossRef](#)]
33. Esteban-Tejeda, L.; Cabal, B.; Torrecillas, R.; Prado, C.; Fernandez-Garcia, E.; López-Piriz, R.; Quintero, F.; Pou, J.; Penide, J.; Moya, J.S. Antimicrobial activity of submicron glass fibres incorporated as a filler to a dental sealer. *Biomed. Mater. (Bristol)* **2016**, *11*, 045014. [[CrossRef](#)] [[PubMed](#)]
34. Beikler, T.; Flemmig, T.F. Oral biofilm-associated diseases: Trends and implications for quality of life, systemic health and expenditures. *Periodontology 2000* **2011**, *55*, 87–103. [[CrossRef](#)] [[PubMed](#)]
35. Bosman, W.M.; Borger van der Burg, B.L.; Schuttevaer, H.M.; Thoma, S.; Hedeman Joosten, P.P. Infections of intravascular bare metal stents: A case report and review of literature. *Eur. J. Vasc. Endovasc. Surg.* **2014**, *47*, 87–99. [[CrossRef](#)] [[PubMed](#)]
36. Dale, H.; Hallan, G.; Hallan, G.; Espehaug, B.; Havelin, L.I.; Engesaeter, L.B. Increasing risk of revision due to deep infection after hip arthroplasty. *Acta Orthop.* **2009**, *80*, 639–645. [[CrossRef](#)] [[PubMed](#)]
37. Yokoe, D.S.; Avery, T.R.; Platt, R.; Huang, S.S. Reporting surgical site infections following total hip and knee arthroplasty: Impact of limiting surveillance to the operative hospital. *Clin. Infect. Dis.* **2013**, *57*, 1282–1288. [[CrossRef](#)] [[PubMed](#)]
38. Parvizi, J.; Pawasarat, I.M.; Azzam, K.A.; Joshi, A.; Hansen, E.N.; Bozic, K.J. Periprosthetic joint infection: The economic impact of methicillin-resistant infections. *J. Arthroplast.* **2010**, *25* (Suppl. 6), 103–107. [[CrossRef](#)] [[PubMed](#)]

